European **J**ournal of **Chem**istry

Check for updates

Response surface optimization and modeling of caffeine photocatalytic degradation using visible light responsive perovskite structured LaMnO₃

Muktar Musa Ibrahim [1],*, Hamza Rabiu Sani [2], Khuzaifa Muhammad Yahuza [3], Aminu Hassan Yusuf [4], and Ahmad Bello Bungudu [5]

[1] *Department of Chemistry, Faculty Science, Ahmadu Bello University, Zaria, 1044, Nigeria*
sagagi1914@gmail.com (M.M.I.)

[2] *Department of Chemistry Faculty of Science, Federal University Dutsen-Ma, 82101, Nigeria*
hrabiu001@gmail.com (H.R.S.)

[3] *Department of Chemistry, Faculty of Science, Abubakar Tafawa Balewa University, Bauchi, 740211, Nigeria*
yahuzakhuzaifa@gmail.com (K.Y.M.)

[4] *School of Physical and Chemical Sciences, University of Canterbury, Christ-Church, 8140, New Zealand*
ahdeocean@yahoo.com (A.H.Y.)

[5] *Cardiff Catalysis Institute, School of Chemistry, Cardiff University, Cardiff, CF10 3AT, UK*
ahmadb4@cardiff.ac.uk (A.B.B.)

* *Corresponding author at: Department of Chemistry, Faculty Science, Ahmadu Bello University, Zaria, 1044, Nigeria.*
e-mail: musa.ibrahim@abu.edu.ng (M.M Ibrahim).

RESEARCH ARTICLE

KEYWORDS

ABSTRACT

Caffeine is a refractory pollutant of emerging concern that evades conventional waste-water treatment techniques. Here, we report the synthesis of visible light responsive perovskite structured LaMnO₃ photocatalyst using modified Pechini method and utilized it as an efficient photocatalyst for caffeine degradation. XRD, BET, UV-Vis, NH₃-TPD, and SEM were used to characterize the photocatalyst. Response surface methodology using Central composite design was used to investigate the effect of three operational variables; catalyst dosage, initial caffeine concentration and pH on the caffeine photocatalytic degradation efficiency. The functional relationship between these operational variables and caffeine photocatalytic degradation efficiency was established be a second order polynomial model. The results of the response surface analysis indicate caffeine degradation efficiency is most significantly affected by catalyst dosage and pH. The optimal values of operational obtained by response surface optimization were found be 3.5 g/L for catalyst dosage, 7.9 and 44.6 mg/L for pH and initial caffeine concentration respectively given the caffeine degradation efficiency of 93.9%.

1. Introduction

Caffeine is pervasive in every part of the world. Typically, caffeine is the main stimulant commonly found in coffee, tobacco, tea, kola and many other carbonated drinks. Caffeine finds its way to the sewage systems from many anthropogenic sources and it tends to persist due to its high solubility and low volatility. Caffeine is classified with other psychoactive substances as emerging pollutants that present a new global water quality challenge with potentially-serious threats to human health and ecosystems [1]. Although the effect of caffeine on human health is mild at low concentrations, serious life-threatening conditions were reported as a result of high intake of caffeine [2]. The widespread occurrence of caffeine in wastewaters, sewage and soil presents a thing of major concern due to its recalcitrant nature [3]. The inability of conventional wastewater treatment technologies to effectively remediate this pollutant of emerging concern prompted scientists and engineers to search for novel solutions [4]. In the last two decades, many different methods and technique have been explored for the remediation of emerging pollutants but none received more attention than the so-called Advance Oxidation Processes (AOPs) [5]. AOPs in wastewater treatment applications generally involves a set of methods and techniques that degrade recalcitrant organic pollutant in aqueous medium by producing highly potent reactive oxidation species *in situ* [6]. The example of these reactive oxidation species (ROSs) include •OH, •O, HO₂•, HO₄• and O₂• [7]. AOPs are commonly employed environmental remediation includes; heterogeneous photocatalysis, Fenton-processes and photo electrocatalysis [8,9].

Advanced oxidation processes are reported to be able to completely mineralize even the most recalcitrant organic pollutants without any environmental footprint [10,11]. In heterogeneous photocatalysis, ROSs are generated by semiconductor

photocatalysts when electrons are excited from the valence band (VB) of a semiconductor photocatalyst to the conduction band (CB) of the photocatalyst upon irradiation by light of a suitable frequency leaving behind a photogenerated hole (h^+). A detailed mechanism for the photodegradation of organic pollutants was discussed elsewhere [6].

Numerous semiconductor photocatalysts have been exploited for their potential in photodegradation applications [12]. Up until now, the most commonly used semiconductors in environmental remediation are the so-called wide-bandgap semiconductors such as TiO_2 and ZnO [13]. However, it was realized that despite their merits such as; high photostability, low cost, and small environmental footprint [14]. The large-scale applicability in photodegradation schemes utilizing wide bandgap semiconductors is seriously hampered. This is because their range of light absorption is limited only to the ultra-violet (UV) region which constitutes a small percentage (4-5%) of entire solar irradiation [15,16]. For more efficient and low-cost utilization photodegradation schemes, the utilization of light in the visible region of the solar spectrum which constitutes about 40-50% of the entire solar spectrum must be considered [17,18].

Some of the methods that have been widely explored to improve the visible light responsiveness of wide-bandgap semiconductors photocatalyst include doping [19], dye sensitization [4,20], and surface property modification [13]. Despite the research efforts been exerted in trying to improve the visible responsiveness of wide-bandgap semiconductor photocatalyst [21]. It can be said that minimal success in large-scale application of photocatalytic degradation is achieved. This is partly because most of the procedures reported to improve the visible responsiveness of wide-bandgap semiconductors are usually complex, costly, and often unreliable [22]. The attention of many scientists is now turning to find better alternatives to wide-bandgap semiconductor photocatalysts. Among the most interesting alternatives considered for application in environmental remediation is the use of perovskite structured oxide semiconductors. Several researchers have investigated the applicability of perovskite structured oxide semiconductors in the photodegradation of recalcitrant organic pollutants [7,14-16].

Perovskite oxides have received increasing attention due to their unique electrical, magnetic, catalytic, and superconductive properties that are utilized in various technological and basic materials science investigations [6,9]. With regards to the use of Perovskite structured oxide semiconductors in photocatalysis, researchers tend to focus mainly on the bandgap, stability, and cost of the semiconductor photocatalyst. Another favorable advantage of perovskite structured semiconductors photocatalyst is the ease with which these materials can be engineered to produce better photocatalysts [3,5]. The ideal perovskite has a cubic structure with a chemical formula of ABX_3 where A and B are cations representing metals in 12- and 6-coordinated sites and X is an anion [18]. Perovskite structured $LaMnO_3$ is a p-type semiconductor consisting of oxygen octahedra with a central Mn atom. $LaMnO_3/Fe_2O_3$ prepared using the co-precipitation method was utilized effectively to degrade methylene blue dye [7]. In another study, perovskite structured $LaMnO_3$ was utilized to effectively degrade rhodamine B dye [23]. Some of the reports indicate the usefulness of perovskite structured $LaMnO_3$ and its modified forms in the photodegradation of various organic dyes [17-23]. Given the successes $LaMnO_3$ recorded as a photocatalyst, it is interesting that little work is done on its utilization as an efficient photocatalyst for the degradation and mineralization of recalcitrant emerging pollutants.

In this work, we give an initial report on the evaluation of perovskite structured $LaMnO_3$ as an efficient photocatalyst for photodegradation of aqueous caffeine using response surface analysis. The morphology and structure of the photocatalyst were investigated using powdered X-ray diffraction, scanning electron microscopy, and Brunauer-Emmet-Teller analysis, and the direct bandgap was determined using Tauc plot. To identify the active sites in the photocatalyst, we carried out an NH_3-TPD analysis. The optimal value of catalyst dosage, initial caffeine concentration, and pH were investigated using Response Surface optimization.

2. Experimental

2.1. Chemicals

$LaNO_3$ (99.5 %), H_2SO_4 (98.08 %) and citric acid were obtained from Loba Chemie, India. $Mn(NO_3)_2$ (99 %) and caffeine were obtained from Sigma Aldrich and BDH Poole, respectively. All the chemicals used in this research were used as received from the manufacturers without further purification. All Stock solutions used in this work were prepared using deionized distilled water and used fresh.

2.2. Synthesis of perovskite structured $LaMnO_3$ photocatalyst

The $LaMnO_3$ perovskite photocatalyst was synthesized via the Pechini method, which utilizes metal nitrates with citric acid as the chelating agent [13]. The Pechini method is a two-stage synthetic process that involves the formation of a complex between the metal ion precursors and citric acid. And then, the complexes formed are mixed and heated to form the perovskite catalyst. Specifically, complexes of La and Mn with citric acid as a chelating agent were formed by mixing the $LaNO_3$ and $Mn(NO_3)_2$ precursors with citric acid in a ratio of 1:4 (metal nitrate precursor to citric acid) under vigorous stirring at a temperature of 60 °C. The pH of the solution was adjusted to 7 using ammonia, and ethylene glycol was added to the thick viscous solution obtained and then heated at 90 °C with stirring. The resin-like substance that was formed after water evaporation was dried at 120 °C overnight in an oven and then Calcined in a muffle furnace at 800 °C for 4 h.

2.3. Photocatalyst characterization

The Powdered X-ray Diffraction (PXRD) pattern of the synthesized $LaMnO_3$ photocatalyst was recorded on a Rigaku Ultima IV diffractometer, equipped with Cu-Kα source (λ = 1.56877 Å). The X-ray tube was operated at 40 kV and 30 mA, and the intensity was recorded over a 2θ range of 20 to 80° and step size of 0.02. Scanning Electron Microscopy (SEM) micrograph was obtained using (Philips XL-30ESM) which is coupled with an energy dispersive spectrometer (EDS). The UV-Vis diffused reflectance spectra (DRS) were obtained from UV-VIS CINCO 4100 and absorbance values used to monitor the photodegradation of caffeine were recorded using a UV-Vis spectrophotometer (Agilent technology, Cary Series). Nitrogen desorption isotherm was obtained using QUARDSORB (Quantum Instruments, USA) apparatus operated at 77.35 K. Before Brunauer-Emmet-Teller isotherm BET measurement. The sample was degassed at 120 °C for 0.5 h. The surface area (S_{BET}) was computed from the adsorption isotherm using the Brunauer-Emmet-Teller equation. The temperature programmed desorption for nitrogen (NH_3-TPD) was carried out by first pre-treating $LaMO_3$ photocatalyst using N_2 (145 mL/min) at 350 °C for 17 h and then cooled to 100 °C.

2.4. Photodegradation experiment

A 400 mL aqueous suspension of a known amount of caffeine and $LaMnO_3$ photocatalyst is added to a quartz photoreactor described in our previous work [4].

Table 1. Experimental factors and levels of operational variables.

Factor	Name	Units	Minimum	Maximum
A	Catalyst load	g/L	2.00	3.50
B	Caffeine concentration	mg/L	20.00	70.00
C	pH	-	3.00	8.00

Table 2. Central composite design matrix and experimental responses.

Run	Catalyst load (g/L)	Initial caffeine concentration (mg/L)	pH	Degradation (%)	Predicted
1	2.00	70	8.0	72	73.0
2	2.75	45	5.5	86	85.0
3	2.75	45	5.5	86	85.0
4	2.00	20	8.0	83	81.0
5	3.50	20	3.0	74	73.5
6	3.50	45	5.5	87	84.0
7	2.75	45	5.5	86	85.2
8	3.50	70	3.0	60	63.0
9	2.75	70	5.5	79	80.0
10	3.50	20	8.0	96	97.0
11	2.00	20	3.0	68	68.5
12	2.00	70	3.0	68	67.0
13	2.75	20	5.5	85	85.7
14	2.00	45	5.5	73	74.0
15	2.75	45	5.5	86	85.0
16	2.75	45	3.0	77	76.3
17	2.75	45	8.0	93	92.3
18	2.75	45	5.5	86	85.0
19	2.75	45	5.5	75	84.6
20	3.50	70	8.0	83	82.8

The aqueous suspension was stirred at 200 rpm for 10 min to harmonize the catalyst-pollutant mixture and allowed to equilibrate in the dark for 30 minutes. After equilibration, the aqueous suspension was exposed to light irradiation (250 W Xe lamp, Osram Germany) which served as the visible light source for photocatalytic activity measurement. 10 mL aliquot was taken at specific time intervals (between 0 and 120 min) and the powdered catalyst was separated by centrifuging a sample at 500 rpm for 30 minutes. The supernatant liquid obtained was filtered using a 0.45 μm cellulose nitrate filter to remove the residual photocatalyst. The residual level of caffeine was monitored by measuring absorbance at 272 nm using a UV-Visible spectrophotometer (Agilent Technology, Cary Series). The photodegradation efficiency of the perovskite structured LaMnO₃ was computed as the percentage (% D) of the initial caffeine concentration and caffeine concentration at time *t* using Equation (1).

$$\%D = \frac{[Caffeine]_0 - [Caffeine]_t}{[Caffeine]_0} \times 100 \tag{1}$$

where $[Caffeine]_0$ is the initial caffeine concentration and $[Caffeine]_t$ is the concentration of caffeine at irradiation time *t*.

2.5. Design of experiment and Response Surface Methodology (RSM)

Preliminary experiments were conducted using the conventional one factor at a time (OFAT) optimization method to discern the most significant factors affecting the photodegradation efficiency and their levels. Based on the results obtained from the preliminary studies, the operational factors: catalysts loading, caffeine concentration, and pH were used to optimize the photodegradation process using Central composite design (CCD) as implemented in Design Expert 11 (StatEase, Inc. USA). The levels of experiments and the design matrix for the CDD are shown in Tables 1 and 2, respectively. The aforementioned operational parameters and the photodegradation efficiency (%D) as a response function were utilized to develop a robust regression model that predicts the values of photodegradation efficiency under different conditions. Finally, we carry out confirmation studies by comparing the results predicted by the regression model and experimental results obtained under the same conditions.

3. Results and discussion

3.1. Structural and morphological characterizations

The structural characteristics of the synthesized LaMnO₃ photocatalyst were evaluated using the XRD diffraction spectrum as shown in Figure 1. The diffraction peaks observed at 23.06, 32.56, 37.71, 40.23, 46.91, 52.31, 57.69, 68.62, and 73.01° Corresponding to (012), (110), (104), (202), (024), (122), (300), (220), (208), (312), and (128) indices can be readily indexed with LaMnO₃ perovskite having rhombohedral phase structure with R-3c space group (COD card No: 1521791). The characteristic peaks in the XRD profile were sharp and distinct, indicating that the synthesized LaMnO₃ photocatalyst synthesized is made of well-formed crystals. The absence of peaks due to MnO or LaO over the whole XRD spectrum clearly shows the homogeneity of the LaMnO₃ photocatalyst. The amount of Mn^{4+} in the crystal lattice of LaMnO₃ tends to determine the phase structure of the crystal [16]. The phase structure of LaMnO₄ is orthorhombic when the concentration of Mn^{4+} in LaMnO₃ crystal is within the range of 0-12% and it becomes rhombohedral and cubic when the concentrations of Mn^{4+} in the LaMnO₃ lattices are 18-3 and >30%, respectively. Given that the theLaMnO₃photocatalysts synthesized in the report have a rhombohedral structure, it can be inferred that the concentration of M^{4+} about 18-20% of the LaMnO₃. Lattice constants obtained after Rietveld analysis of the LaMnO₃XRD diffraction data were $a = b = 5.5310$ Å and $c = 13.3630$ Å with a unit cell volume of 354.0315 Å³.

SEM micrograph and EDX spectrum of the synthesized LaMnO₃ is shown in Figure 2. It is observed from the EDX spectra (Figure 2a), that the major constituent elements of the synthesized LaMnO₃ photocatalyst are the substituted elements (La: 58.97%, Mn: 24.31%) and oxygen (19.28%). Another prominent peak due to carbon is also observed which is attributed to the carbon-coated copper grip used in a typical EDX machine.

The SEM micrograph (Figure 2b) indicates that the as-synthesized LaMnO₃ particles were irregular in shape and highly agglomerated. The clumping of the LaMnO₃ photo-catalyst might be attributable to their magnetic nature. The specific surface area of a photocatalyst plays an important role in its activity since it increases the contact area between the pollutant's particles and the photocatalyst.
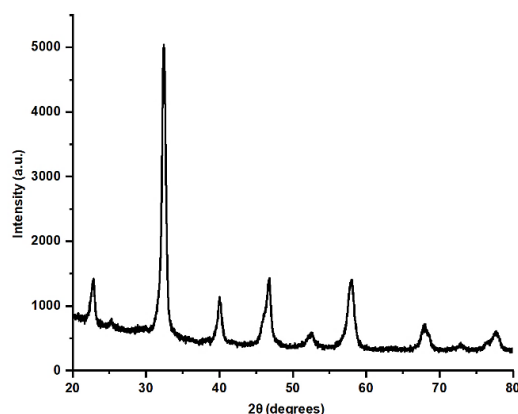
Figure 1. PXRD profile of the synthesized LaMnO₃ at calcined at 800 °C.
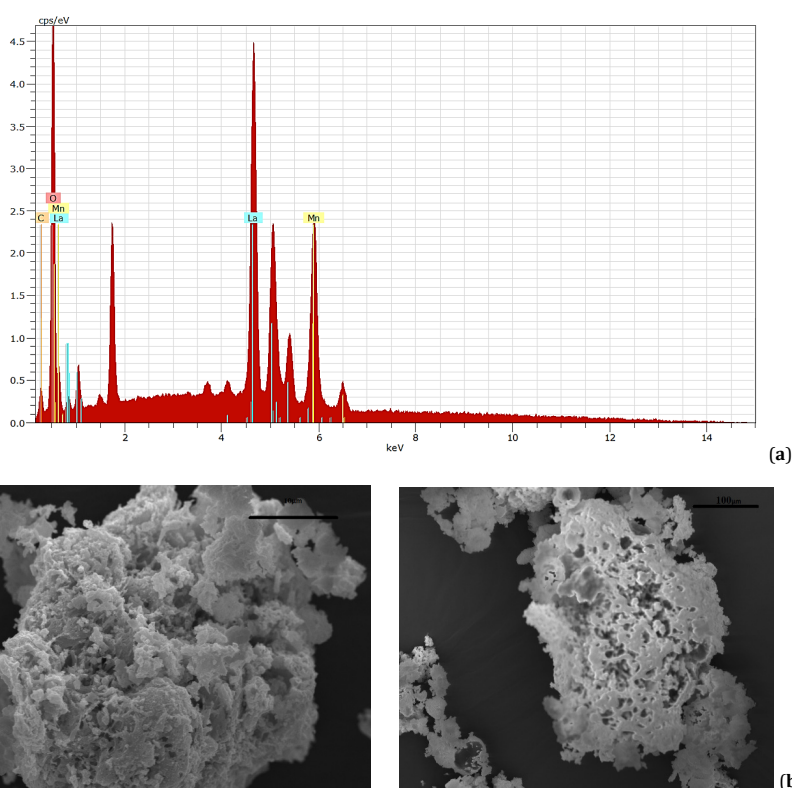

Figure 2. (a) EDS analysis of as-synthesized LaMnO₃ and (b) SEM micrograph of synthesized LaMnO₃.

As a general rule of thumb, the higher the surface area the more active a photocatalyst will be as a result of an increase in surface for adsorption [21]. The BET isotherm and corresponding BET plot of LaMnO₃ photocatalyst are shown in Figure 3. The BET isotherm (Figure 3a) can be described as a typical type IV isotherm Considering the IUPAC classification. This type of isotherm indicates the formation of monolayer at the lower region, which is a characteristic of meso-porous materials (pore diameter; 2-50 nm). Using the BET plot as shown in Figure 3b, the specific surface area of the LaMnO₃ photocatalyst was computed with the BET equation to be 68.566 m²/g. The BET surface area of LaMnO₃ photocatalyst reported in this study is significantly higher than the 25.0 m²/g value reported in the literature [21-26] The discrepancy might be attributed to the differences in solvents, and the calcination temperature used in the photocatalyst synthesis. The higher specific surface area is a good indicator of the activity of the photocatalyst. The higher surface area means that more

caffeine is absorbed on the photocatalyst surface Thereby, increasing the probability of contact between the photocatalyst and caffeine molecules.

The acidic property of the perovskite structured LaMnO₃ was investigated using temperature-programmed desorption of ammonia (NH₃-TPD) between 100-900 °C as shown in Figure 4. The NH₃-TPD profile was obtained by raising temperature linearly with time while a steady stream of NH₃ flows through the sample. At a certain temperature, the thermal energy overcomes the activation energy, and the bond between the sample and NH₃ breaks. The three broad peaks at 322, 495, and 641 °C observed in Figure 4 indicate the existence of three different active sites on the LaMnO₃ photocatalyst. The three active sites include one weakly acidic (< 400) and two strongly acidic sites. The presence of an acidic active site in the LaMnO₃ photocatalyst will facilitate the adsorption of caffeine on its surface given its basic nature. Hence, improving the overall caffeine photocatalytic degradation efficiency.
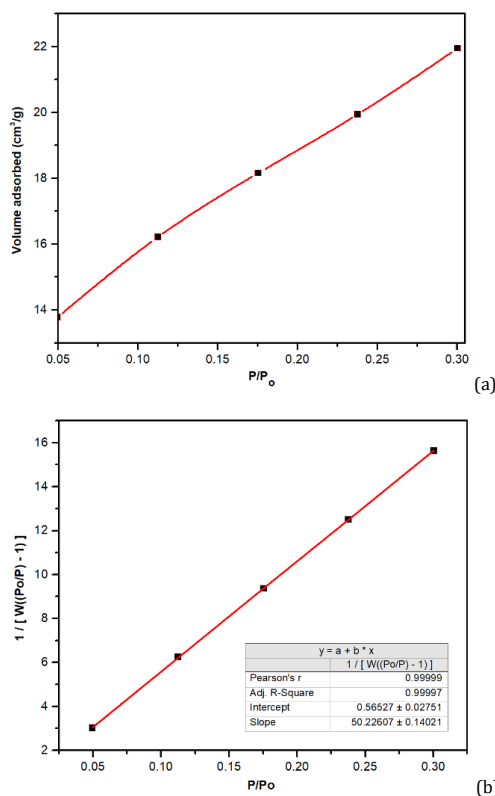
Figure 3. (a) BET isotherm of LaMnO₃ photocatalyst calcined at 800 °C and (b) BET plot of LaMnO₃.
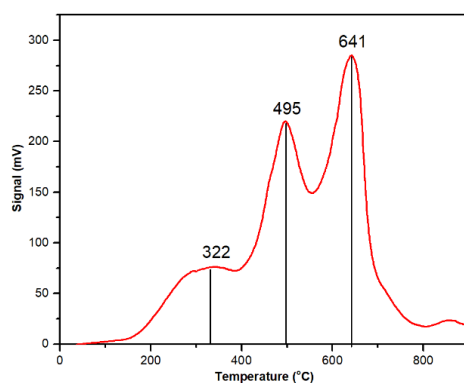

Figure 4. NH₃-TPD Isotherm of Perovskite structured LaMnO₃ photocatalyst.

The bandgap is an important material property in photocatalysis. It determines whether a photocatalyst is active in a particular region of the electromagnetic spectrum or not. The UV-VIS absorption spectrum and Tauc plot (inset) of the synthesized LaMnO₃ photocatalyst is shown in Figure 5. It is observed that the spectrum has a very strong absorption peak at about 312 nm which is attributable to charge-transfer interaction between O^{2-} and Mn^{3+} in the photocatalyst [14]. The bandgap (E_g) of the LaMnO₃ photocatalyst was determined using the Tauc equation (Equation (2)). The direct bandgap value E_g can be extrapolated by fitting a straight to the linear segment to intersect the $h\nu$ axis from the plot of $(\alpha h\nu)^2$.

$$\alpha h\nu = A(h\nu - E_g)^n \tag{2}$$

where $h\nu$ the photon energy in eV is, α is absorption coefficient, E_g is the direct bandgap, A is a proportionality constant and n is either 2 or ½ for direct and indirect transitions respectively. The value of the direct bandgap of LaMnO₃ obtained from the Tauc plot (inset, Figure 6) was 2.88 eV. This indicates that the photocatalyst is visible light-responsive. This value is consistent with the literature value of 2.82 eV for pure LaMnO₃ synthesized using the sol-gel method [18]. The discrepancies between the band gap value and the value reported [19] might be attributed to the crystallite size difference between the catalysts.

3.2. Response surface analysis and numerical optimization

3.2.1. Preliminary studies

The levels of operational parameters used for response surface design were determined from one factor at time (OFAT) optimization of the independent parameters. In the OFAT optimization scheme, the optimal photocatalytic degradation efficiency is obtained for a chosen independent variable while keeping other variables constant.
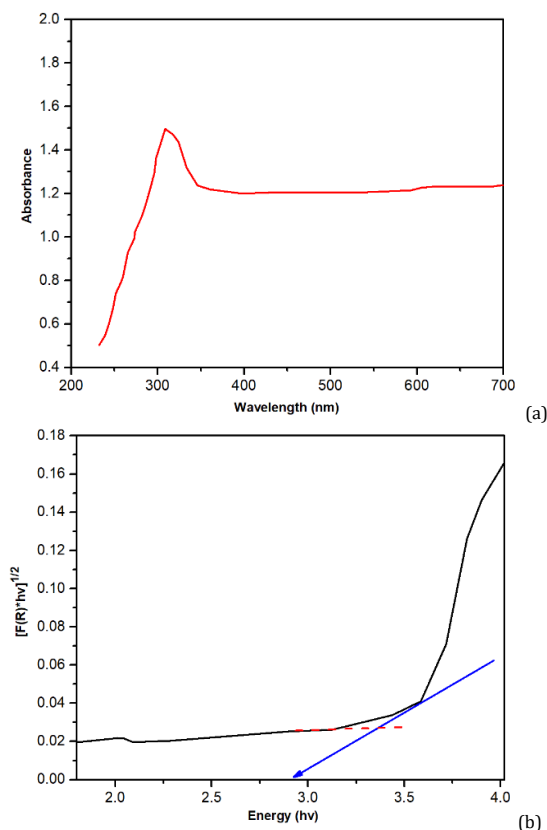
Figure 5. (a) UV-Visible spectra and (b) Tauc plot of LaMnO$_3$ photocatalyst.

The results obtained for the effect of different catalyst dose 0.5-10 g/L on caffeine photocatalytic degradation is shown in Figure 6a. It is observed that the rate of caffeine degradation increases from 15 to 55% by increasing the amount of the LaMnO$_3$ photocatalyst from 0.5 to 2 g/L. The increase in photodegradation efficiency with increase in catalyst load is due to greater availability of the active site for the photocatalytic degradation. However, an optimal catalyst load was attained at 2 g/L, beyond which an increase in catalyst dose does not increase the photocatalytic degradation efficiency. This might be attributable to increase in turbidity of the system at higher catalyst load, which hampers light penetration [11].

The effect of pH on the photocatalytic degradation of caffeine is shown in Figure 6b. The rate of the photocatalytic degradation of caffeine by perovskite structured LaMnO$_3$ photocatalyst also increases with increasing pH in the acidic medium. The pH range with the highest photocatalytic degradation efficiency was observed in the neutral and slightly basic pH region. Due to its basicity, it will be more soluble in low pH aqueous solutions than in high pH solutions. This is because in low pH solutions, caffeine would exist completely as a protonated salt, making it more hydrophilic. Despite this, caffeine is very polar and is still quite soluble in water at higher pH levels This indicate that caffeine molecules were more stable in acidic medium less stable in basic medium. The initial caffeine concentration was varied at constant catalyst load and pH to studied to study its effect of the degradation efficiency. Figure 6c show that the rate of removal of caffeine decreases at higher initial concentrations with the highest degradation efficiency obtained at concentration of 40 mg/L. The reduced photodegration efficiency observed with higher levels of caffeine concentrations might be attributed to lack of catalysts sites [4].

3.2.2. Model fitting and statistical analysis

Experimental design matrix and experimental responses conducted at different levels of independent variables for the photodegradation of caffeine using LaMnO$_3$ photocatalyst are shown in Table 2. The best model that describes the empirical relationship between the operational parameters; pH, initial caffeine concentration, and catalyst dosage, and caffeine degradation was established to be a second-order polynomial equation based on actual values as shown in Equation (3).

% Degradation = -13.977 + 52.0667×(Catalyst load) + 0.705152×(Caffeine conc.) + -0.106667×(pH) + -0.106667×(Catalyst load)×(Caffeine conc.) + 1.73333×(Catalyst load)×(pH) + -0.02×(Caffeine conc.)×(pH) + 9.45455×(Catalyst load)^2 + -0.00530909×(Caffeine conc.)^2 + -0.0509091×(pH)^2

$$(3)$$

The adequacy and the statistical significance of the model (Equation (3)) are checked using analysis of variance (ANOVA) and results obtained for the second-order polynomial model are shown in Table 3.

It is observed from Table 3 that the overall model p-value (0.0006) is less than the level of significance (0.05). Therefore, the null hypothesis, that there is no relationship between caffeine degradation and the three operational variables is rejected. There is only a 0.06% chance that F-value this large could occur due to noise. The p-values of linear terms for all the operational variables are also lower than the level of significance indicating that they significantly affect caffeine photodegradation. The quadratic terms of the operational variables are found to be insignificant with a p-value greater than the level of significance.

Table 3. ANOVA results of the second-order polynomial model and independent variables.

Source	Sum of squares	df	Mean square	F-value	p-value
Model	1411.54	9	156.84	9.990	0.0006
A-Catalyst load	129.600	1	129.60	8.250	0.0166
B-Caffeine concentration	193.600	1	193.60	12.33	0.0056
C-pH	640.000	1	640.00	40.76	< 0.0001
AB	32.0000	1	32.000	2.040	0.1839
AC	84.5000	1	84.500	5.380	0.0428
BC	12.5000	1	12.500	0.796	0.3932
A^2	77.7800	1	77.780	4.950	0.0502
B^2	30.2800	1	30.280	1.930	0.1951
C^2	0.27840	1	0.2784	0.017	0.8967
Residual	157.010	10	15.700		
Lack of fit	56.1800	5	11.240	0.557	0.7318
Pure error	100.830	5	20.170		
Corrected total sum of square	1568.55	19			
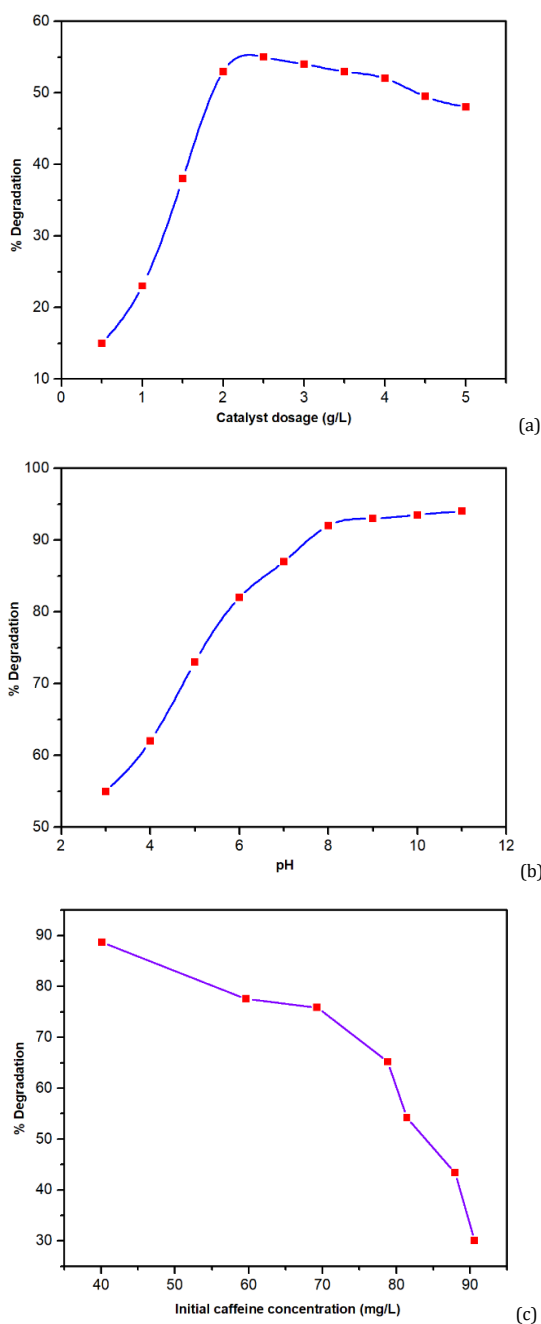
Figure 6. Effect of operational parameters on the caffeine photocatalytic degradation (a) effect of catalyst dosage, (b) effect of pH and (c) effect of initial caffeine concentration.
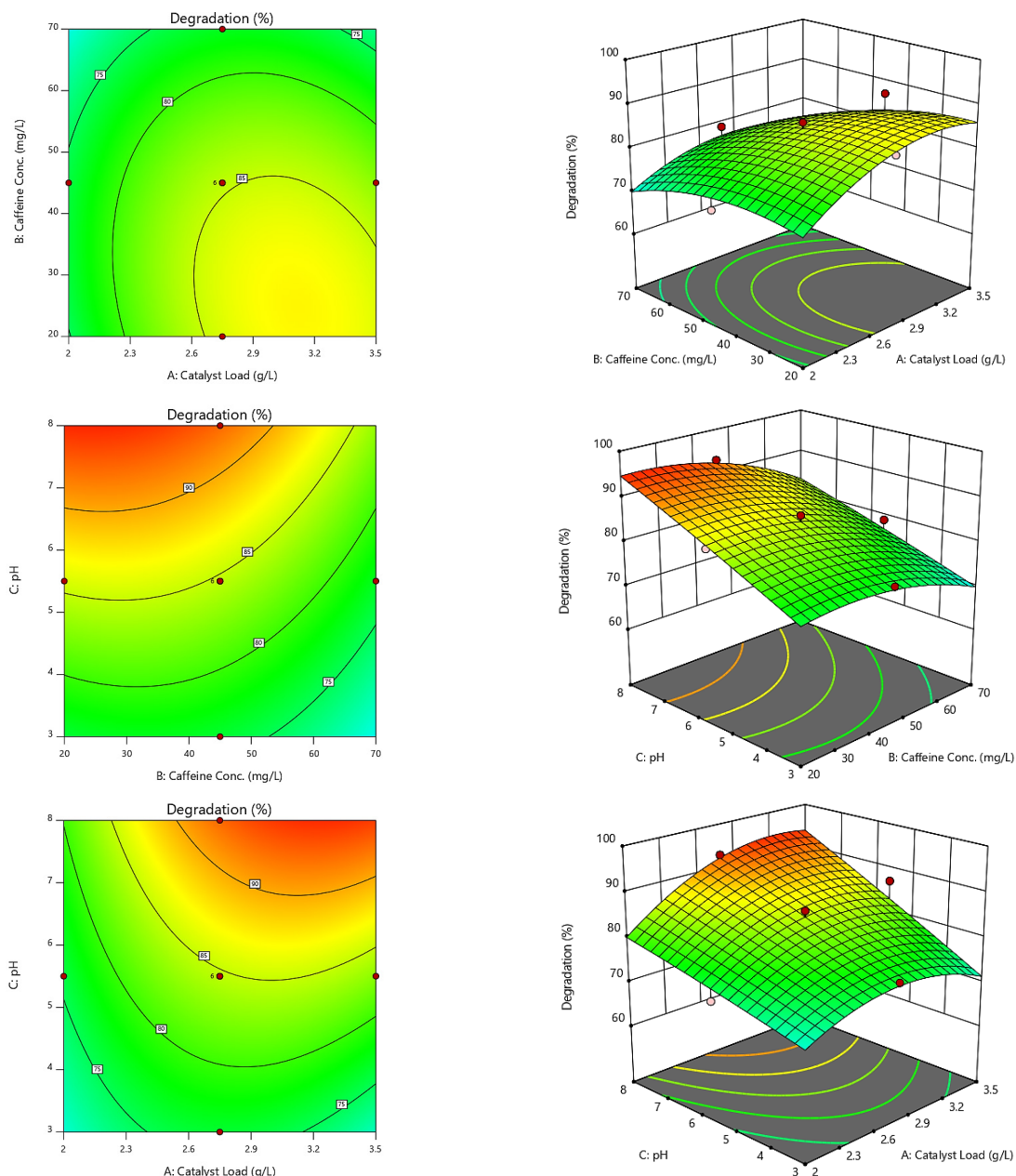
Figure 7. Response surface and contour plots.

The model suffers no lack of fit because the model lack fit p-value (0.7318) is larger than the level of significance (0.05). Therefore, the quadratic model with the predictor variables; catalyst dosage, initial caffeine concentration, and pH is adequate to predict the caffeine degradation. The adjusted R^2 value of 91% indicates that the model parameters can explain variations in independent variables. The R^2 value of 0.917 shows good agreement between values predicted by the model and the values measured experimentally. The signs and the value of the regression coefficients of the second-order polynomial model (Equation (3)) represent the expected change in response per unit change in the value of independent parameters used in the model. The sign of the coefficient of each operational variable indicates its direction of change while the coefficient values indicate the strength of the relationship. The linear coefficient value of catalyst loading of 3.60 indicates that if all other variables are held constant in the model, the caffeine degradation will increase by 3.60 if the catalyst load is increased by 3.6 g/L. The negative sign of the regression

coefficient of initial caffeine concentration shows that as it has a negative effect on caffeine degradation. The positive influence of the increased number of $LaMnO_3$ active sites on the process kinetics as the catalyst load increases is indicated by the positive value of the regression coefficient for catalyst load. However, at higher catalyst loading a slight decrease of caffeine photodegradation was observed. Because, even though the availability of active sites increases with catalyst loading, but there is reduced light penetration, and hence, the photo-activated volume of the suspension shrinks. Similar observations have also been reported in other studies on various organic substances [22].

3.2.3. Response surface analysis

Response surface analysis has been utilized as a powerful technique to optimize the effect of operational parameters in photocatalytic degradation of recalcitrant organic pollutants.
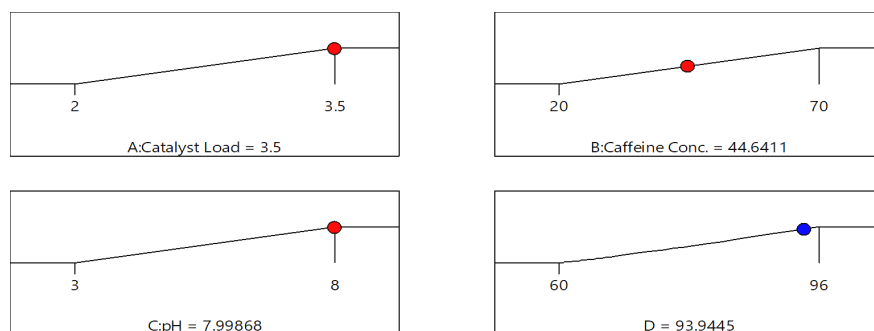
Figure 8. Ramp for numerical optimization of caffeine photocatalytic degradation using perovskite structured LaMnO₃.

The interactions between operational parameters and response at different levels are given visually represented by the 3D response surface plot. The 3D surface plot and corresponding 2D contour plot of the effect of catalyst load, initial caffeine concentration, and pH are shown in Figure 7. The surface plots give a graphical representation of the effect of changing operational variables on the response. It is observed in Figure 7a that the caffeine degradation increases linearly as the levels of pH change from 3 to 8. However, the effect of catalyst dosage on caffeine degradation increases from 2 to 3 g/L beyond which the caffeine degradation decreases steadily. This is because the initial increase in catalyst dosage up to the optimum dosage increases the number of active sites for caffeine degradation. Beyond the optimum catalyst dosage, a decrease in caffeine degradation is observed due to decreased light penetration as the suspension becomes cloudier. The red-colored region in the contour plot represents the maxima of the response surface plot. Optimal caffeine degradation is predicted from the contour plot to occur at pH = 7-8 and catalyst dosage of 2.5-3 g/L. Caffeine degradation decreases with an increase in initial caffeine concentration whereas it increases with an increase in catalyst loading as shown in Figure 7b. The region that represents the highest caffeine degradation when these parameters are considered is when the catalyst loading is about 2.7 g/L and the initial caffeine concentration is 50 mg/L. The surface plot for the interaction between pH and initial caffeine concentration as shown in Figure 6c shows that caffeine degradation increases linearly with pH and there no significant interaction between the two variables. This is supported by the p-value (0.3932) of their linear interactions which was greater than the level of significance (0.05).

3.3. Numerical optimization

The main objective of RSM is optimization, finding the best set of factor levels to achieve some goal. Here, the factor level combinations that give the maximum caffeine photocatalytic degradation efficiency were obtained using a numerical optimization algorithm as implemented by Design-Expert software. Since the goal of our RSM optimization is to get the highest photocatalytic degradation efficiency, the highest importance (+++++) for the goal (Maximize) was chosen to obtain the best possible values of operational parameters. The factory settings for optimal caffeine photocatalytic degradation recommended by the numerical optimization are pH value of 8, an initial caffeine concentration of 44.6 mg/L, and catalyst dosage of 3.5 g/L as shown in Figure 8. Under these conditions, the predicted response was 93.944%.

3.4. Model validation analysis

The suitability of a model is confirmed when the prediction interval of the model is in agreement with the sample average.

The adequacy of our model was tested by a conducting photocatalytic degradation experiment in three replicates using the factor setting recommended by numeral optimization. The mean caffeine photocatalytic degradation efficiency was found to be 92.81% which is inside the prediction interval of the model. The agreement between the experimental value and predicated value indicates that our model can be used to simulate photocatalytic degradation of caffeine using LaMnO₃.

4. Conclusion

Response surface analysis of the photocatalytic degradation of caffeine using perovskites structured LaMnO₃ was carried out. The photocatalytic degradation process was found to be responsive to the operational parameters; pH, Initial caffeine concentration, and catalyst dosage. A mathematical model that best describes the relationship between the operational parameters and photocatalytic degradation efficiency was found to be a second-order polynomial equation. Using Numerical optimization based on desirability function, the optimal conditions for the photodegradation process were found to be a pH value of 8, an initial caffeine concentration of 44.6 mg/L, and catalyst dosage of 3.5 g/L.

Disclosure statement DS

Conflict of interests: The authors declare that they have no conflict of interest.
Author contributions: All authors contributed equally to this work.
Ethical approval: All ethical guidelines have been adhered.
Sample availability: Samples of the compounds are available from the author

ORCID iD

Muktar Musa Ibrahim
iD https://orcid.org/0000-0002-8250-5074
Hamza Rabiu Sani
iD https://orcid.org/0000-0001-5329-0601
Khuzaifa Muhammad Yahuza
iD https://orcid.org/0000-0002-0792-8421
Aminu Hassan Yusuf
iD https://orcid.org/0000-0002-3650-1697
Ahmad Bello Bungudu
iD https://orcid.org/0000-0003-0761-880X

References

[1]. Geissen, V.; Mol, H.; Klumpp, E.; Umlauf, G.; Nadal, M.; van der Ploeg, M.; van de Zee, S. E. A. T. M.; Ritsema, C. J. *Int. Soil Water Conserv. Res.* **2015**, *3* (1), 57–65.

[2]. Nawrot, P.; Jordan, S.; Eastwood, J.; Rotstein, J.; Hugenholtz, A.; Feeley, M. *Food Addit. Contam.* **2003**, *20* (1), 1–30.

[3]. Moore, M. T.; Greenway, S. L.; Farris, J. L.; Guerra, B. *Arch. Environ. Contam. Toxicol.* **2008**, *54* (1), 31–35.

[4]. Ibrahim, M. M.; Gaya, U. I. *J. Chil. Chem. Soc.* **2019**, *64* (1), 4275–4284.

[5]. Sahoo, C.; Gupta, A. K. *J. Hazard. Mater.* **2012**, *215–216*, 302–310.

[6]. Kumar, A.; Kumar, S.; Krishnan, V. Perovskite-Based Materials for Photocatalytic Environmental Remediation. In *Environmental Chemistry for a Sustainable World*; Springer International Publishing: Cham, 2019; pp 139–165.

[7]. Susanti, Y. D.; Afifah, N.; Saleh, R. Comparison between Photo- and Sono- Catalytic Activities of LaMnO3/Fe3O4/NGP to Remove Methylene Blue from Wastewater; AIP Conference Proceedings, 1–6, 2018. Available online: https://doi.org/10.1063/1.5064033

[8]. Gaya, U. I. *Eur. J. Chem.* **2011**, *2* (2), 163–167.

[9]. Sujatha, G.; Shanthakumar, S.; Chiampo, F. *Environments* **2020**, *7* (6), 47.

[10]. Barrocas, B.; Neves, M. C.; Conceicao Oliveira, M.; Monteiro, O. C. *Environ. Sci. Nano* **2018**, *5* (2), 350–361.

[11]. Wang, Y.; Wang, Y.; Yu, L.; Wang, J.; Du, B.; Zhang, X. *Chem. Eng. J.* **2019**, *368*, 115–128.

[12]. Vu, A.-T.; Tuyet Pham, T. A.; Tran, T. T.; Nguyen, X. T.; Tran, T. Q.; Tran, Q. T.; Nguyen, T. N.; Van Doan, T.; Vi, T. D.; Nguyen, C. L.; Nguyen, M. V.; Lee, C.-H. *Bull. Chem. React. Eng. Catal.* **2020**, *15* (1), 264–279.

[13]. Dhiman, T. K.; Singh, S. *Phys. Status Solidi (a)* **2019**, *216* (11), 1900012.

[14]. Ghiasi, E.; Malekzadeh, A. *J. Inorg. Organomet. Polym. Mater.* **2020**, *30* (7), 2789–2804.

[15]. Abdolrahmani, M.; Parvari, M.; Habibpoor, M. *Cuihua Xuebao/Chin. J. Catalysis* **2010**, *31* (4), 394–403.

[16]. Shaterian, M.; Enhessari, M.; Rabbani, D.; Asghari, M.; Salavati-Niasari, M. *Appl. Surf. Sci.* **2014**, *318*, 213–217.

[17]. Abdullah, E. A. *Eur. J. Chem.* **2019**, *10* (1), 82–94.

[18]. Hu, J.; Ma, J.; Wang, L.; Huang, H. *J. Alloys Compd.* **2014**, *583*, 539–545.

[19]. Hu, J.; Ma, J.; Wang, L.; Huang, H.; Ma, L. *Powder Technol.* **2014**, *254*, 556–562.

[20]. Azfar, A. K.; Kasim, M. F.; Lokman, I. M.; Rafaie, H. A.; Mastuli, M. S. *R. Soc. Open Sci.* **2020**, *7* (2), 191590.

[21]. Pei, Z.; Wang, P.; Li, Z. *Eur. J. Chem.* **2019**, *10* (1), 7–11

[22]. Sakkas, V. A.; Islam, M. A.; Stalikas, C.; Albanis, T. A. *J. Hazard. Mater.* **2010**, *175* (1–3), 33–44.

[23]. Arandiyan, H.; Wang, Y.; Scott, J.; Mesgari, S.; Dai, H.; Amal, R. *ACS Appl. Mater. Interfaces* **2018**, *10* (19), 16352–16357.